# Generation, shaping, and characterization of intense femtosecond pulses tunable from 3 to 20 $\mu$m

**Robert A. Kaindl, Matthias Wurm, Klaus Reimann, Peter Hamm, Andrew M. Weiner,* and Michael Woerner**

*Max-Born-Institut für Nichtlineare Optik und Kurzzeitspektroskopie, Max-Born-Strasse 2A, 12489 Berlin, Germany*

Received April 25, 2000; revised manuscript received August 2, 2000

We report on an intense mid-infrared light source that provides femtosecond pulses on a microjoule energy level, broadly tunable in the 3–20-$\mu$m wavelength range with pulse durations as short as 50 fs at 5 $\mu$m. The pulses are generated by phase-matched difference-frequency mixing in GaSe of near-infrared signal and idler pulses of a parametric device based on a 1-kHz Ti:sapphire amplifier system. Pulse durations are characterized with different techniques including autocorrelation measurements in $AgGaS_2$, two-photon absorption in InSb, and cross-correlation measurements with near-infrared pulses in a thin GaSe crystal. A subsequent zero-dispersion stretcher of high transmission allows for optimum pulse compression, a more detailed amplitude and phase characterization and, ultimately, amplitude shaping of the mid-infrared pulses. © 2000 Optical Society of America [S0740-3224(00)00212-5]

*OCIS codes:* 320.7110, 190.2620, 190.4970, 320.5540, 190.7220, 230.4320.

## 1. INTRODUCTION

Femtosecond pulses in the mid-infrared (MIR) spectral range ($\lambda = 3-20\,\mu$m) provide powerful tools to study the ultrafast dynamics of nonequilibrium excitations in condensed matter.[1] Recently, structural changes in molecules or molecular complexes were monitored directly in the time domain by means of the transient absorption of prominent molecular vibrations.[2] Vibrational dynamics and correlations in liquid water or in proteins have been successfully studied with femtosecond pulses in the MIR.[3–6] Femtosecond infrared spectroscopy has also been increasingly applied to problems in solid-state physics.[7] For instance, time-resolved investigations of the coherent[8] or incoherent[9] dynamics of intersubband excitations in semiconductor nanostructures have provided new insights that cannot be obtained by experiments based on interband transitions. Recently the ultrafast dynamics of the electronic system in a high-transition-temperature superconductor was investigated near the conductivity gap with femtosecond MIR pulses as a probe.[10] Such experiments increasingly call for sources that provide intense pulses on the microjoule level with pulse durations of the order of 100 fs or less. In this temporal range tabletop laser systems based on parametric devices are superior to free-electron lasers, which typically provide much longer pulses and for which the realization of synchronized pulses at two different wavelengths is a difficult problem that involves additional high-power laser systems.

Here we demonstrate a novel setup that pushes the generation of intense MIR femtosecond pulses close to its limits. In noting that one optical cycle at $\lambda = 15\,\mu$m amounts to 50 fs, we find that the pulses generated in our setup consist of only approximately three optical cycles, in close analogy to the shortest pulses (≈5-fs-duration) generated in the near infrared.[11–13] In what follows, we give a brief overview of the available setups, focusing on the long-wavelength schemes

*$\lambda = 2$–$5\,\mu m$* Sources for this limited range are comparatively abundant. Such setups permit, for example, the generation of as much as 100 mW of 60–150-fs pulses from high-repetition-rate (80-MHz) parametric oscillators based on $KNbO_3$ or $KTiOAsO_4$ (KTA) crystals.[14,15] At kilohertz repetition rates, parametric amplification in KTP provides equally short pulses down to ≈70-fs duration with 200-nJ pulse energy in the 3–4-$\mu$m range.[16] Difference-frequency mixing of signal and idler pulses in thin KTP or $LiIO_3$ crystals generates 200-fs pulses tunable from 2.5 to 5 $\mu$m.[17–20]

*$\lambda = 3$–$10\,\mu m$* This broader range necessitates use of nonlinear crystals with sufficient transparency. The limited number of possible materials includes $AgGaS_2$ (Table 1) or $ZnGeP_2$. Difference mixing of the output of an 82-MHz, two-color Ti:sapphire laser in $AgGaS_2$ permitted the generation of 500-fs pulses tunable from 7.5 to 12.5 $\mu$m.[21] At low repetition rates, a $ZnGeP_2$-based parametric amplifier produces 200-fs pulses ($\lambda = 6\,\mu$m) tunable from 2.5 to 10 $\mu$m.[22] From amplified Ti:sapphire laser systems that deliver intense pulses at a 1-kHz repetition rate, 130-fs pulses tunable from 3 to 10 $\mu$m were generated by difference-frequency mixing (DFM) pulses from an optical-parametric amplifier (OPA) in $AgGaS_2$.[23,24]

*$\lambda = 10$–$20\,\mu m$* Generation of femtosecond pulses at wavelengths beyond 10 $\mu$m has barely been studied. Complex setups constructed from 80-MHz parametric oscillators and subsequent DFM in $AgGaSe_2$ or GaSe deliver output powers of ≤2 mW in the 5–18-$\mu$m range.[25,26] However, from such schemes that combine several nonlinear frequency-conversion stages and require high-power Ti:sapphire lasers (1–2 W) and synchronously pumped,

 

**Table 1. Properties of Various Nonlinear Crystals**[a,b]

| Crystal | Point Group | Transmission Range ($\mu$m) | $\lambda_{REF}$ ($\mu$m) | Nonlinear Coefficient (pm/V) | Effective Nonlinearity $d_{eff}$ | $n_o$ | $n_e$ |
|---|---|---|---|---|---|---|---|
| $KH_2PO_4$ (KDP) | $\bar{4}2m$ | 0.17–1.5 | 1 | 0.39 ($d_{36}$) | $d_{ooe} = d_{36} \sin\theta \sin 2\phi$<br>$d_{eoe} = d_{36} \sin 2\theta \cos 2\phi$ | 1.50 | 1.46 |
| ($\beta$-$BaB_2O_4$) (BBO) | $3m$ | 0.19–3 | 1 | 2.3 ($d_{22}$)<br>0.16 ($d_{31}$) | $d_{ooe} = d_{31} \sin\theta - d_{22} \times \cos\theta \sin 3\phi$<br>$d_{eoe} = d_{22} \cos^2\theta \cos 3\theta$ | 1.66 | 1.54 |
| $LiIO_3$ | 6 | 0.28–6 | 1 | 4.4 ($d_{31}$) | $d_{ooe} = d_{31} \sin\theta$ | 1.86 | 1.72 |
| $AgGaS_2$ | $\bar{4}2m$ | 0.47–13 | 10 | 12 ($d_{36}$) | $d_{ooe} = d_{36} \sin\theta \sin 2\phi$<br>$d_{eoe} = d_{36} \sin 2\theta \cos 2\phi$ | 2.35 | 2.30 |
| $AgGaSe_2$ | $\bar{4}2m$ | 0.71–19 | 10 | 33 ($d_{36}$) | $d_{ooe} = d_{36} \sin\theta \sin 2\phi$<br>$d_{eoe} = d_{36} \sin 2\theta \cos 2\phi$ | 2.59 | 2.56 |
| CdSe | $6mm$ | 0.75–25 | 10 | 18 ($d_{31}$) | $d_{oeo} = d_{31} \sin\Theta$ | 2.43 | 2.45 |
| GaSe | $\bar{6}2m$ | 0.62–20 | 10 | 54 ($d_{22}$) | $d_{ooe} = d_{22} \cos\theta \sin 3\phi$<br>$d_{eoe} = d_{22} \cos^2\theta \cos 3\phi$ | 2.70 | 2.38 |
| Te | 32 | 3.5–36 | 10 | 670 ($d_{11}$) | $d_{eeo} = d_{11} \cos^2\theta \sin 3\phi$<br>$d_{oeo} = d_{11} \cos\theta \cos 3\phi$ | 4.79 | 6.25 |

[a] Refs. 35 and 36.

[b] Nonlinear coefficients and refractive indices are listed for $\lambda_{REF}$. The indices of effective nonlinearity $d_{abc}$ denote the polarizations ($o$, ordinary; $e$ extraordinary) of phase-matched process $a + b \rightarrow c$.

stabilized external cavities, only pulse durations above 300 fs were demonstrated. Recently, some of the present authors and others demonstrated a compact scheme for the generation of pulses of typically ≈150-fs duration in the spectral range from 7 to 20 $\mu$m at high repetition rates by parametric mixing within the broad spectra of 13-fs pulses from a 2-MHz cavity-dumped Ti:sapphire oscillator in GaSe.[27] Setups based on amplified systems allow for much higher pulse energies but typically produce even longer pulses. Bayanov *et al.*[28] use the second harmonic of a 4-Hz, 7-mJ picosecond Nd:glass amplifier to pump a three-path OPA. By subsequent DFM in GaSe, pulses tunable from 4 to 20 $\mu$m and with energies of as much as 11 $\mu$J are generated. Their pulses (700-fs duration) are to our knowledge the shortest that have been demonstrated from an amplified system in the 10–20-$\mu$m spectral range. Other setups generate pulses of 1-ps (Ref. 29) or 10-ps (Ref. 30) duration. Recently it was shown that non-phase-matched optical rectification of very short, ≈10-fs Ti:sapphire pulses or optically switched high-field transport in semiconductors can also provide higher-frequency components up to the MIR ($\lambda > 8$ $\mu$m) range.[31–34] However, applications to nonlinear (e.g., pump–probe) spectroscopy with such an ultrabroadband (0–30 THz) source are rare because of the large spectral spread of group delay and diffractive properties and the very low (nanowatt) average powers. In summary, until now the wavelength range beyond 10 $\mu$m was much less explored for very short pulses, of the order of 100 fs.

An essential problem for the generation of intense MIR pulses by DFM exists in the competing process of two-photon absorption in the nonlinear crystal. To prevent this process from occurring, the shortest wavelength of the two incident waves must be at least twice the wavelength that corresponds to the electronic absorption edge of the nonlinear crystal. Unfortunately, nonlinear crystals that are transparent in the MIR spectral range (e.g., $AgGaS_2$, $AgGaSe_2$, GaSe...; cf. Table 1 and Refs. 35 and 36) have their absorption edges in the visible or the near infrared and thus exclude the attractive possibility of using amplified Ti:sapphire laser systems directly for pumping DFM. The established method for high-power, femtosecond DFM is the two-stage parametric setup that was also used in our experiments.

In this paper we present a comprehensive study of the generation, shaping, and characterization of tunable few-cycle pulses of MIR light ($\lambda \approx 3-20$ $\mu$m). Our setup is based on a 1-kHz regenerative amplifier and uses optical parametric amplification followed by DFM in GaSe. It covers the 3–20-$\mu$m spectral range with large pulse energies of as much as 1 $\mu$J and pulse durations as short as 50 fs. In addition, we apply pulse shaping and several characterization techniques to explore further the limits of MIR femtosecond pulse generation. The paper is organized as follows: First we present our experimental setup with the focus on the crucial elements for the generation of ultrashort electric field transients. Then we characterize the spectral and temporal properties of the MIR pulses. Finally, we discuss various applications of a MIR zero-dispersion stretcher that allows for optimum pulse compression, more-detailed amplitude and phase characterization and, ultimately, amplitude shaping of the MIR pulses.

## 2. EXPERIMENTAL SETUPS AND PULSE SPECTRA

We describe our home-built multistage setup that generates high-intensity MIR femtosecond pulses at a repetition rate of 1 kHz. The primary stage consists of a regenerative amplifier (Quantronix Model 4800 RGA) that delivers 90-fs pulses with 500 $\mu$J of energy at 800-nm wavelength. In further stages the pulses are converted into near-infrared signal and idler pulses ($\lambda$

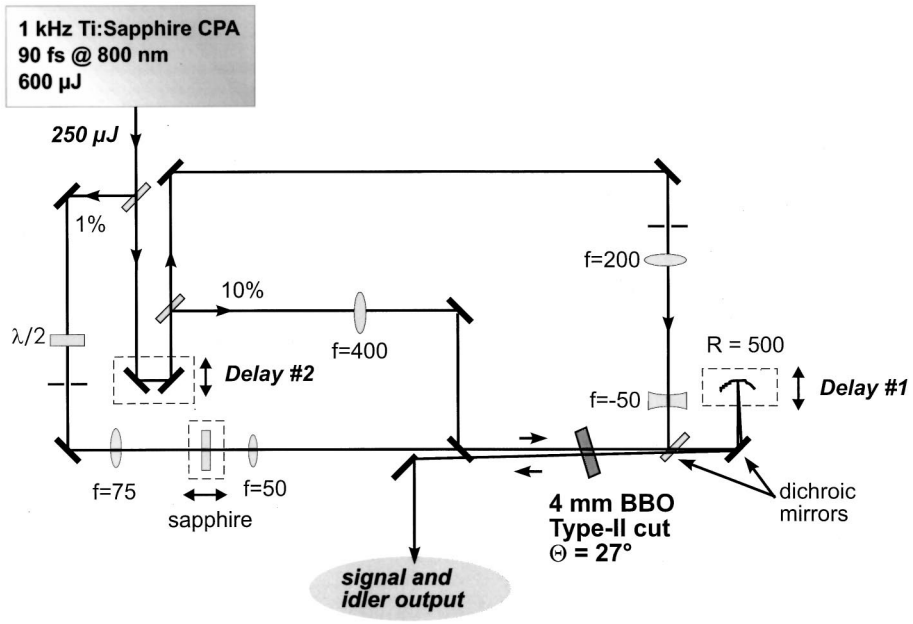


Fig. 1. Two-stage OPA for the generation of tunable femtosecond signal and idler pulses in the near infrared ($\lambda = 1$–$2\ \mu$m). In the actual setup, the beams for the first and second stages are slightly displaced in height rather than sideways. CPA, chirped pulse amplification; other abbreviations defined in text.

$\approx$ 1.2–2.4 $\mu$m) by optical parametric amplification. Finally, DFM in a GaSe crystal generates the desired MIR pulses tunable in the 3–20-$\mu$m spectral range.

Our home-built two-stage $\beta$-$BaB_2O_4$ (BBO) OPA is similar to that used in the research reported in Ref. 24 and is shown schematically shown in Fig. 1. To pump the OPA, only half the output power of the regenerative amplifier is needed; the second half provides additional synchronized pulses to the experiment. We generate seed pulses by focusing a small portion ($\approx$1%) of the amplified 800-nm pulses into a sapphire plate (thickness, $d = 1$ mm), thus generating a white-light continuum. Next, the seed pulses and 10% of the temporally delayed pump pulses (Delay #2 in Fig. 1) are spatially and temporally overlapped and focused into the 4-mm BBO amplifier crystal. The type II process used here fulfills the phase-matching conditions $\omega_{\text{pump}} n_{eo}(\omega_{\text{pump}}, \Theta) = \omega_{\text{signal}} n_o(\omega_{\text{signal}}) + \omega_{\text{idler}} n_{eo}(\omega_{\text{idler}}, \Theta)$ and $\omega_{\text{pump}} = \omega_{\text{signal}} + \omega_{\text{idler}}$, in which $n_o(\omega)$ and $n_{eo}(\omega, \Theta)$ denote the frequency-dependent refractive indices for ordinary and extraordinary polarization, respectively. Tilting the BBO crystal for optimal phase-matching angles ($\Theta \approx 27°$) generates ~700 nJ of signal and idler output during this first stage of amplification.

For the second amplification step, suitable dichroic mirrors[37] remove the undesired idler and residual Ti:sapphire components from the first stage. The remaining signal beam is then collimated by a concave mirror (radius, $R = 50$ cm), which also serves as a temporal delay for the second pass (Delay #1, Fig. 1). The signal pulses are steered back into the same BBO crystal at a slightly different height. Using the same crystal for both amplifier stages simplifies tuning. The fresh and intense pump pulses ($\approx$200 $\mu$J) used in the second amplification step pass through a telescope, which adapts their beam size to the 2-mm diameter of the collimated signal beam.

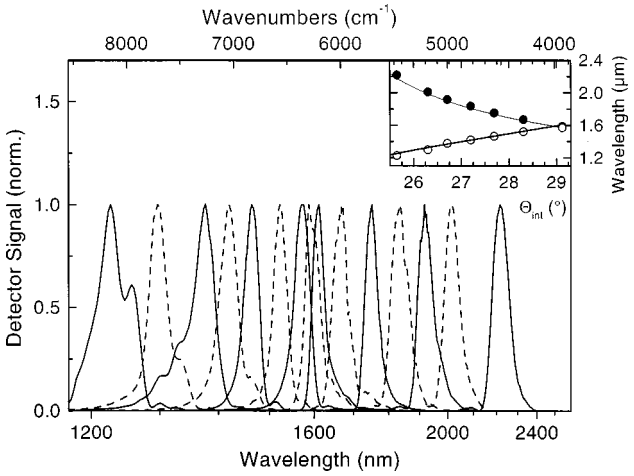


Fig. 2. Normalized spectra of signal and idler pulses generated in the 1-kHz two-stage type II BBO OPA. The spectra are acquired with a 0.22-m grating monochromator and a 300 line/mm grating. Inset, experimental tuning characteristics of idler (filled circles, extraordinary polarization) and signal (open circles, ordinary polarization) and calculated phase-matching curve (internal angles) for a Ti:sapphire pump wavelength of $\lambda = 795$ nm.

Pump pulses and signal pulses are overlapped temporally and spatially and propagate unfocused through the BBO crystal, generating intensive signal and idler pulses. The OPA delivers intense near-infrared pulses at its output with pulse energies (sum of signal and idler) of approximately 70–80-$\mu$J across the whole tuning range. Because the amplifier is operated in the saturation limit, small pulse-to-pulse fluctuations of $<$1% are achieved.

Spectra of the signal and idler pulses were measured with a grating spectrometer and an InAs detector and are shown in Fig. 2. The signal and idler pulses are continuously tunable in the wavelength range from 1.2 to 2.4 $\mu$m

with negligible adjustments. Pulse durations were measured by noncollinear autocorrelation with a 100-$\mu$m BBO crystal and a Si diode. Pulse durations of 90–120 fs (signal) and 80–120 fs (idler) were determined in this way across the entire tuning range.

It is important to note that the use of type II phase matching here entails significant advantages: first, the OPA can be tuned to the degeneracy point of 1.6 $\mu$m, ultimately permitting the generation of small difference frequencies. Second, the signal and idler polarizations are oriented perpendicularly and thus are already correctly aligned for the subsequent difference-frequency process.

In the final generation stage, the MIR pulses are generated by DFM of signal and idler in a 1-mm thick, type I–oriented GaSe crystal for which the setup shown in Fig. 3 was used.[37] The temporal overlap is adjusted with a delay stage that separates signal and idler pulses by use of broadband dichroic mirrors. A telescope generates an effective focal length of 700 mm, which leads to signal and idler foci of $\approx$500 $\mu$m at the GaSe crystal.

We have chosen GaSe for DFM for the following reasons: a suitable nonlinear material for parametric frequency generation of MIR pulses must fulfill some unconventional criteria. These include large transparency at both pump and output wavelengths, high nonlinearity, suitable birefringence, and a high damage threshold. In addition, two-photon absorption at all interacting wavelengths should be small. Correspondingly, the number of available crystals is small. Several crystals (including some for near-infrared applications) are listed in Table 1. GaSe fulfills all the aforementioned criteria. As GaSe cannot be polished to appreciable quality, it is currently available only with the surface cleaved along the [001] direction. Because of small internal phase-matching angles near 10°, however, a cleaved surface is acceptable for the experiments. However, recent research with indium-doped GaSe shows that crystals cut at arbitrary angles may soon be commonly available.[38]

Adjusting GaSe and BBO crystal angles to appropriate values yields type I phase matching. The energy of the MIR output is measured directly with a sensitive thermopile detector. Pulse energies are very large (1 $\mu$J) near $\lambda = 5$ $\mu$m and fall off almost proportionally to the photon energy at longer wavelengths, corresponding to an essentially constant quantum efficiency of $\approx$10% throughout the entire tuning range.

Beyond the crystal, residual signal and idler components are suppressed by suitable long-pass interference filters with onset wavelengths in the MIR. A reference beam is split off with a KBr plate and overlaps a fixed He–Ne adjustment laser with mirrors M1 and M2 and two apertures. In this way, steerability of the invisible MIR beam throughout the rest of the setup is accomplished.

The pulses are tunable in a wide spectral range from 3 to 20 $\mu$m, as is demonstrated in Fig. 4(a) for several settings of the BBO and GaSe phase-matching angles. Interestingly, in GaSe the phase-matching curves for DFM and for MIR second-harmonic generation (SHG) intersect at 36° [Fig. 4(b)]. At this setting, simultaneous generation of pulses near $\lambda = 7-8$ $\mu$m and $\lambda = 4$ $\mu$m is achieved. Thus the generation of intense and synchronized pulses at two different MIR wavelengths in a single crystal becomes possible [open circles in Fig. 4(a)]. When this effect is not desired, a simple interference filter removes the second harmonic. The dual-wavelength opera-

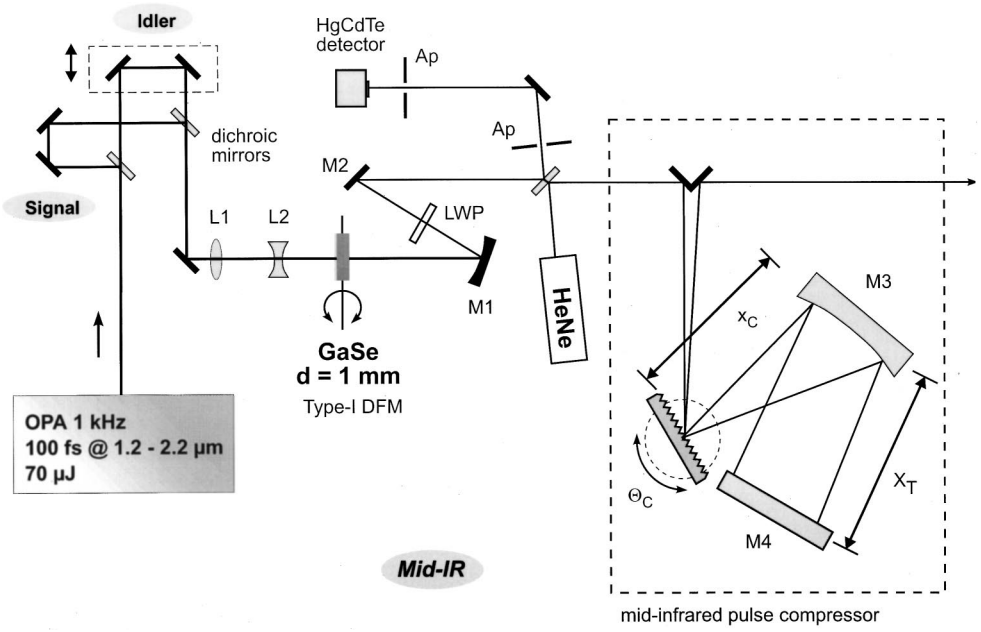


Fig. 3. Setup for DFM and subsequent compression and shaping of femtosecond MIR pulses. Broadband dichroic mirrors reflect the signal and transmit the idler pulses. The lenses in the telescope have focal lengths $f = 150$ mm (L1) and $f = -100$ mm (L2) and a spacing of 100 mm. The generated MIR (Mid-IR) beam is collimated by mirror M1 and transmitted through a long-wave-pass filter (LWP). A KBr plate oriented at a 22° angle of incidence splits off ~5% of the incident light and transmits it through two apertures (Ap's). Optionally, a pulse compressor can be inserted, which is constructed from a gold-coated grating (75 lines/mm), a spherical gold-coated mirror (M3; diameter, 3″; $f = 8$″), and a backfolding gold-coated mirror (M4). In the actual setup, M4 is located above the grating to minimize astigmatism.

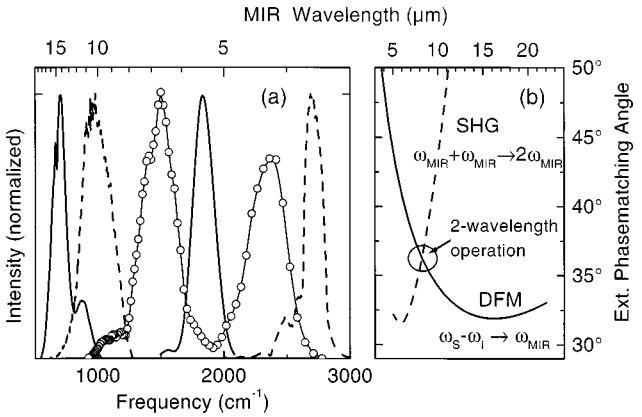


Fig. 4. (a) Spectra of 1-kHz MIR femtosecond pulses for several phase-matching angles. The spectra are acquired with a 0.22-m grating monochromator and HgCdTe detectors. Suitable gratings with 75, 100, and 300 lines/mm, depending on the spectral range, were used. The very broad tuning range is evident from the figure. In relevant spectral ranges, particularly near 6 $\mu$m, we remove $CO_2$ and water absorption in air by purging the setup with $N_2$. (b) Calculated phase-matching angles for DFM (OPA, 1.6-$\mu$m degeneracy point) of signal and idler and for SHG of the MIR pulses in GaSe.

tion shows that the MIR intensity is strong enough to produce significant conversion efficiency at the second harmonic. Thus for two-color operation at other MIR wavelengths a second GaSe can serve for SHG. Alternatively, a second synchronized source can be constructed from an identical setup because only half of the output of the regenerative amplifier is needed for each IR source.

## 3. TEMPORAL CHARACTERIZATION OF MID-INFRARED PULSES

Now we discuss various techniques for the temporal characterization of our femtosecond MIR pulses. Because the GaSe dispersion is small in the near infrared, short MIR pulse durations might be anticipated from our generation scheme. Further handling and characterization of these MIR pulses at wavelengths larger than $\lambda > 10\ \mu$m, however, present a problem because the dispersion of most materials increases strongly in that range. Therefore, different methods optimized for each specific spectral position are applied.

Autocorrelation is comparatively simple and is used for the shorter wavelengths below 10 $\mu$m. For these autocorrelation measurements the MIR pulses are split into two beams by a broadband beam splitter, which consists of a KBr wedge plate onto which a thin transmittive gold layer has been sputtered. One of the beams is temporally delayed by a motorized scanning stage. The beams are recombined, but with a small vertical displacement, and are then focused onto the nonlinear medium. The angle chosen between the incident noncollinear beams is small ($\approx 4°$) but is large enough to prevent significant linear interference between the two beams. Other nonlinear effects can be used in the autocorrelation measurements, as is demonstrated in Fig. 5: In the first case, SHG in a 1-mm-thick $AgGaS_2$ crystal is chosen, with phase-matching angles near 20°–40° for type I phase matching in the wavelength range $\lambda \approx 3-7\ \mu$m. Interference filters are used to block off any fundamental light on the detector. Pulse widths of only 54 fs are measured at $\lambda = 5.5\ \mu$m [Fig. 5(a)], which represents an optimal time–bandwidth product of only $\Delta v \Delta t = 0.34$ (close to the theoretical limit for a sech$^2$-shaped pulse). This extremely short duration, which is below even the incident signal and idler durations, can be explained by the occurrence of the zero-dispersion point near $\lambda = 5\ \mu$m in GaSe. Under such conditions, temporal gain narrowing, i.e., pulse shortening during the conversion process, can occur.[39] $AgGaS_2$ becomes unfavorable for characterizing pulses at wavelengths $\lambda > 7\ \mu$m, because the phase matching angles vary strongly as a function of wavelength, hence limiting the bandwidth. Ultimately, phase-matching of SHG breaks down beyond $\approx 10.5\ \mu$m. Similar arguments apply for autocorrelation measurements by sum-frequency mixing with other crystals such as GaSe and Te.

In an intermediate wavelength range ($\lambda = 7-11\ \mu$m) a second type of autocorrelation measurement becomes useful that is based on two-photon absorption in a thin (250-$\mu$m) InSb crystal. At room temperature, InSb exhibits a bandgap of 0.18 eV ($\lambda = 6.9\ \mu$m). The InSb dispersion in this range gives a dispersion length of approximately 0.6–1 mm for an incident 100-fs pulse. For the measurements, the induced two-photon absorption on the probe beam is measured after selection of this beam with an aperture. The result of a measurement at $\lambda = 9.6\ \mu$m is shown in Fig. 5(b). The pulse duration of 108 fs gives a time–bandwidth product of $\Delta v \Delta t = 0.85$.

Upconversion is useful for pulse characterization, especially for $\lambda > 10\ \mu$m. It is based on sum–frequency mixing of weak MIR and strong OPA signal pulses in a thin GaSe crystal, which generates pulses shifted to higher photon energy in the near infrared. Effectively, upconversion represents a cross-correlation measurement. The setup is shown in Fig. 6. Approximately 8% of the (*s*-polarized) signal pulses are split off from a $BaF_2$ wedge plate located after the OPA. After the pulses pass through a collimating lens, a motorized scanning stage permits adjustment of the pulse delay (Upconversion Delay, Fig. 6).

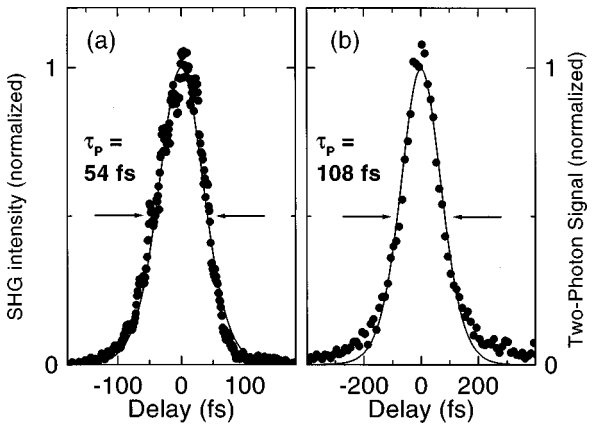


Fig. 5. Autocorrelation traces at (a) $\lambda = 5.5\ \mu$m, measured by SHG in $AgGaS_2$, and at (b) $\lambda = 9.6\ \mu$m, measured by two-photon absorption in InSb. Symbols, experimental data; curves, sech$^2$ fits with pulse width $\tau_p$.

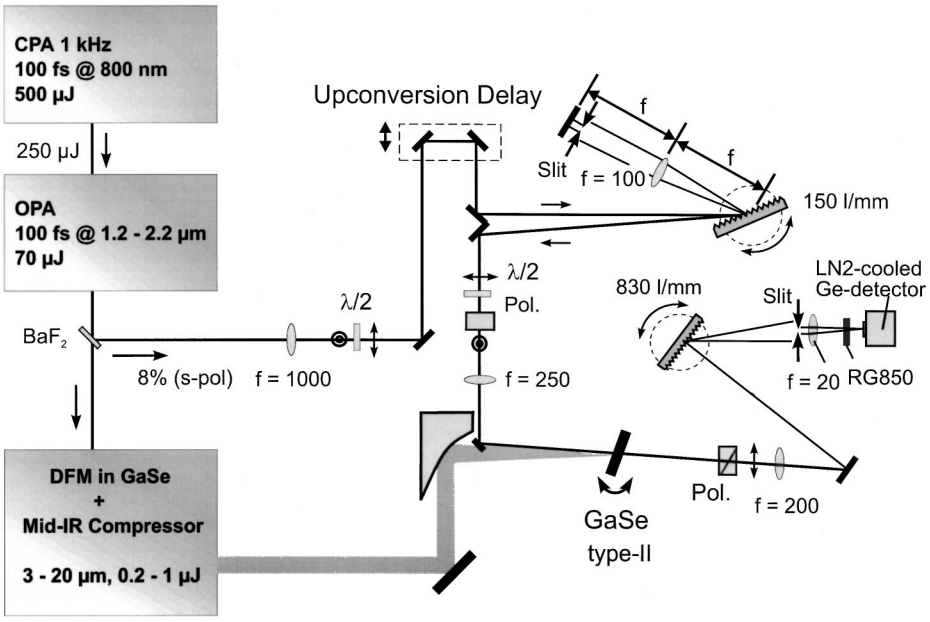


Fig. 6. Setup for temporal characterization of femtosecond MIR pulses using upconversion. It is based on type II sum-frequency mixing of weak MIR and strong OPA signal (gate) pulses in a thin GaSe crystal. The gate pulses are preshaped in a zero-dispersion stretcher unit containing an appropriate slit to suppress background photons already present at the sum frequency. Pol.'s, polarizers; CPA, chirped pulse amplification; other abbreviations defined in text.

As the sum-frequency beam generated in upconversion is weak compared with the incoming near-infrared beam, several measures are taken to ensure the former beam's detectability. The high-frequency wing of the signal pulses already contains photons at this sum frequency; to remove these background photons it is necessary to use an extremely well-defined, rectangularly shaped bandpass filter. This sharp cutoff is not available from any interference filters and is accomplished with a grating-based pulse shaper.[40] This configuration contains a 150-line/mm (l-mm) grating blazed at $\lambda = 1.2\,\mu$m, an $f = 100$-mm lens, and a mirror that reflects the beam back into itself (see Fig. 6). Distances equal to the lens's focal length are chosen that lead to a negligible influence on the pulse duration (zero-dispersion stretcher).[41–43] Because the spectrum is split up in the focal plane (mirror), a positionable slit directly in front of the mirror selects the desired wavelength interval and cuts off any other light. To minimize losses at the grating, the signal polarization is turned perpendicularly to the grooves before it enters the pulse shaper. A broadband polarizer ensures clean polarization of the beam before it enters the upconversion crystal. The signal beam is focused into the GaSe crystal with an $f = 250$-mm lens. To find the spatial overlap with the MIR beam we use a HgCdTe detector with a small area ($250 \times 250\,\mu$m), which can be repositionably placed at the GaSe location, for prealignment.

The GaSe crystal is oriented for type II phase matching, so MIR and near-infrared photons add up to a new sum photon shifted to higher energies: $\omega_{\mathrm{MIR}}(e) + \omega_{\mathrm{OPA}}(o) \rightarrow \omega_{\mathrm{SUM}}(e)$ where $o$ and $e$ denote ordinary and extraordinary polarizations, respectively. This weak upconverted signal is separated from the incoming, much stronger near-infrared beam by polarization and spectral selection with an 830-line/mm grating. The photons are detected by a highly sensitive, low-noise $LN_2$-cooled Ge detector, which permits measurement of extremely small near-infrared powers of as little as ≈3 pW.

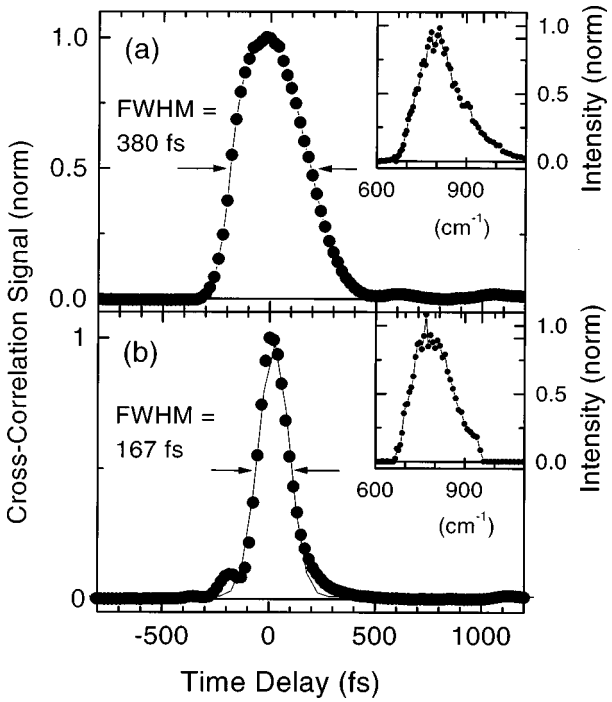


Fig. 7. Cross-correlation traces of femtosecond MIR pulses ($\lambda = 12.5\,\mu$m) before the introduction (a) of the pulse shaper and (b) of optimally compressed pulses afterward. Insets, the corresponding pulse spectra, which show a bandwidth of ≈150 $\mathrm{cm}^{-1}$. The numbers denote the FWHM of the cross-correlation trace. Deconvolution with a 120-fs signal pulse duration yields MIR pulse durations of (a) 360 and (b) 115 fs, assuming Gaussian shaped pulses, yielding time–bandwidth products of $\Delta\nu\Delta t = 0.5$ with the pulse compressor and $\Delta\nu\Delta t = 1.5$ without.

For this sensitivity a separation of greater than $1{:}10^8$ of the two near-infrared beams is provided by the setup. MIR upconversion experiments with a 1-mm-thick GaSe crystal yield photon conversion efficiencies of $\approx 2 \times 10^{-3}$. This in turn means that extremely weak femtosecond MIR transients with only $\approx$100 fJ of pulse energy can be cross correlated. An example of pulse characterization by upconversion is shown in Fig. 7(a) for $\lambda = 12.5\,\mu$m. Here a 65-$\mu$m-thick GaSe layer (which we obtained by gluing a thicker crystal onto fused silica and stripping off the top layers with Scotch tape) is used for upconversion to prevent any lengthening through group-velocity mismatch. The upconversion trace is deconvoluted with the 120-fs signal pulse. For simplicity a Gaussian-shaped pulse is assumed, for which a simple deconvolution expression is known: $\tau_{P,1}^2 + \tau_{P,2}^2 = \tau_{P,\mathrm{CC}}^2$, where $\tau_{P,1}$ and $\tau_{P,2}$ are the pulse durations of the two input pulses and $\tau_{P,\mathrm{CC}}$ is the corresponding duration of the generated cross-correlation signal (FWHM). Thus the deconvolved pulse duration here is 360 fs, which is far from the bandwidth limit. For these longer wavelengths, pulse lengthening can occur already, as a result of dispersion in the GaSe crystal and subsequent optics. Thus we anticipate even shorter pulse durations when subsequent pulse compression is applied.

## 4. PULSE COMPRESSION AND SHAPING

Pulse compression and shaping are implemented here in the MIR for the first time to our knowledge and permit direct control over the phase parameters of the pulse. Inasmuch as this spectral range is governed by negative group-velocity dispersion (GVD) from most materials, a suitable compressor must introduce positive GVD. Thus a simple "Fork prism pair" arrangement, which is often used in the near-infrared, becomes useless because its geometrical effects induce only negative GVD.[44]

The presence of negative GVD necessitates the use of combined angular dispersive and focusing elements, leading to the grating-based arrangement shown in Fig. 3.[42] The incoming beam is spectrally dispersed by the grating. At the outset, the distances $X_C$ and $X_T$ are chosen to be equal to the focal length $f$ of the spherical mirror, such that each spectral component is focused onto a different position on the back mirror (M4 in Fig. 3). This zero-dispersion stretcher configuration has no influence on the pulse duration. However, when the distance of the grating to the spherical mirror is changed to $X_C = f + Z$, the arrangement introduces different path lengths for the various spectral components,[41] which leads to the following expression for the induced GVD:

$$D_\omega = \frac{-4\pi^2 c}{\omega^3 d^2 \cos^2\beta} 2Z, \tag{1}$$

where $\beta$ is the diffraction angle at the pulse's center wavelength $\omega$ and $d$ is the groove spacing of the grating.[41,42] Thus one obtains positive GVD by decreasing $X_C$.

Figure 7(b) shows the result of introducing the pulse compressor into the setup and optimizing $X_C$ for the shortest pulse duration at a wavelength of 12.5 $\mu$m. Quite obviously, the pulse is significantly shorter than the uncompressed pulse in Fig. 7(a). This shorter pulse gives a MIR pulse duration of $\tau_p = 115$ fs and results in a time–bandwidth product of $\Delta\nu\Delta t = 0.5$, very close to the theoretical limit. Considering that one optical cycle at $\lambda = 12.5\,\mu$m amounts to $\approx$40 fs, we find that this pulse duration corresponds to only $\sim$3 cycles of the electrical field.

The compressor also allows more information to be gained about the pulse phase than is available from autocorrelation or cross-correlation measurements. To obtain this information we make an upconversion measurement with a slit placed in front of folding mirror M4 (Fig. 3). Then we can select a finite frequency interval (the slit width corresponds to $\Delta\nu \approx 40\,\mathrm{cm}^{-1}$ in our experiment), which can be scanned across the spectrum. Whereas spectral narrowing automatically broadens the temporal profile, the wavelength dependence of the profile's temporal shift gives a good account of the chirp that is present in the pulse. Such measurements with an optimally compressed pulse are shown in Fig. 8(a), which exhibits only low phase variation. For comparison, the results of shortening $X_C$ by 600 $\mu$m (cf. Fig. 3) are given in Fig. 8(b). Here, a strong (up-)chirp is clearly seen on the pulse, which now corresponds to an overcompressed pulse.

Finally, we want to discuss briefly first experiments for controlled pulse shaping of our MIR pulses. Because the pulse is spectrally dispersed at the back mirror (M4 in Fig. 3), the pulse compressor effectively carries out a

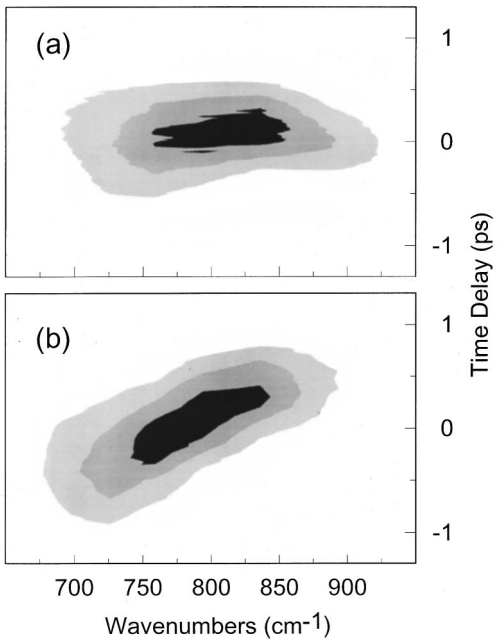


Fig. 8. Two-dimensional intensity profile of wavelength- and time-dependent upconversion signals. The gray scale of the contour plots goes linearly in equidistant steps from 0 (white) to the maximum (black) of the respective intensity profile. Spectral filtering is used with a slit inserted at the back mirror of the compressor. The slit width corresponds to a spectral resolution of $\Delta\nu \approx 40\,\mathrm{cm}^{-1}$. Traces are given for (a) a nearly optimally compressed pulse and (b) a pulse with the compressor length $X_C$ significantly shortened by 600 $\mu$m.

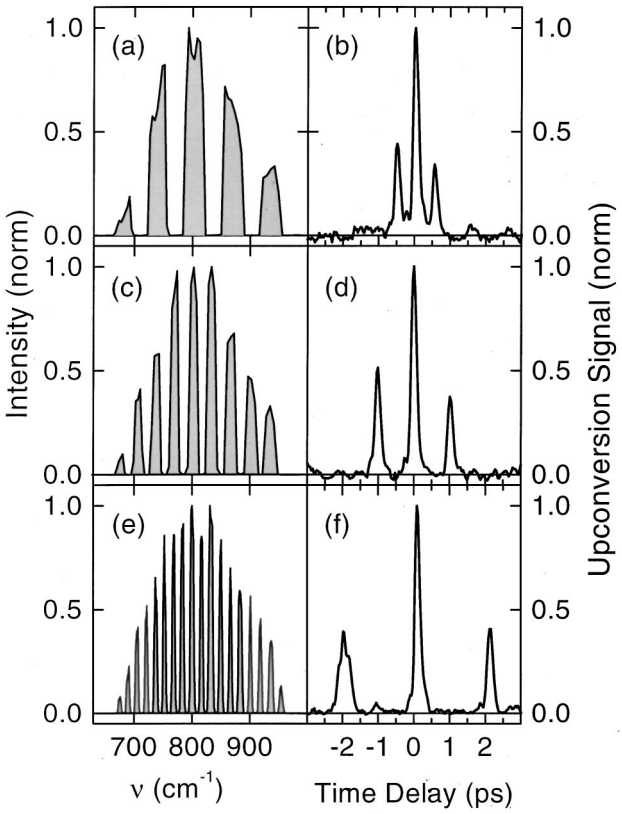


Fig. 9. Spectra (left) and cross-correlation measurements (right) of amplitude-shaped femtosecond MIR pulses with a center wavelength of $\lambda = 12.5\,\mu$m. Cross-correlation traces are obtained by upconversion (i.e., sum-frequency mixing) with near-infrared signal pulses ($\lambda = 1.5\,\mu$m) within a $d = 65$-$\mu$m-thick GaSe crystal. The data are shown for frequency spacings of (a), (b) $\Delta\nu = 66\,\mathrm{cm}^{-1}$; (c), (d) $\Delta\nu = 33\,\mathrm{cm}^{-1}$; (e), (f) $\Delta\nu = 16.5\,\mathrm{cm}^{-1}$. A constant duty cycle of 1:1 between light and dark portions in the spectra is maintained for all measurements.

Fourier transformation (and a backtransformation) of the pulse, which we can exploit to perform manipulations in Fourier space by shaping the amplitude or the phase of the spectrum close to mirror M4. Such pulse-shaping techniques have been successfully applied for many years in the visible and the near-infrared[45–47] but have not yet been extended to the MIR. Here we demonstrate as a first step amplitude shaping of the MIR pulses. For this, patterned amplitude masks with constant frequency spacing are placed directly in front of mirror M4. Figure 9 shows results of amplitude-shaped MIR femtosecond pulses. The spectra of an optimally compressed $\lambda = 12.5\,\mu$m pulse with different spacings of the amplitude pattern (duty cycle 1:1) are shown at the left, with the respective upconversion profiles at the right. New pulses are created by the shaping process. As the frequency spacing decreases from 66 to 16.5 $\mathrm{cm}^{-1}$, the interpulse distance increases in accordance with the Fourier theorem. Currently, experiments with more-powerful techniques for phase shaping of the pulses by adaptive optics are under way and will open new possibilities for coherent control experiments for low-energy transitions in semiconductor nanostructures and vibrations in molecules.

## 5. CONCLUSIONS

In conclusion, we have demonstrated a kilohertz source of intense, approximately 50–150-fs, mid-infrared pulses with a tuning capability from 3 to 20 $\mu$m. Near-infrared signal and idler pulses ($\lambda = 1$–$2\,\mu$m) are generated in a two-pass, type II $\beta$-$BaB_2O_4$ optical parametric amplifier pumped by 250 $\mu$J, from a 1-kHz, 800-nm Ti:sapphire regenerative amplifier. The OPA delivers 100-fs pulses (approximately 70–80-$\mu$J total energy of signal and idler pulses), which are subsequently difference-frequency mixed in a 1-mm-thick, type I oriented GaSe crystal. The pulses are continuously tunable from 3 to 20 $\mu$m. Quantum efficiencies of $\approx$10% are generally measured, yielding the largest pulse energies ($\approx 1\,\mu$J) for short wavelengths. Pulse durations are determined from autocorrelation measurements in a 1-mm-thick $AgGaS_2$ crystal (second harmonic) or in InSb (two-photon absorption). Pulse widths of only 54 fs are measured at the short-wavelength side that originate from temporal gain narrowing in GaSe. Pulses of only $\approx$120-fs duration are obtained for longer wavelengths ($\lambda > 8\,\mu$m) by upconversion. In this spectral range pulse compression is necessary to compensate for dispersion that occurs in the GaSe crystal. Controlled amplitude shaping of our MIR pulses has been demonstrated in new experiments.

## ACKNOWLEDGMENTS

The authors gratefully acknowledge support from the Deutsche Forschungsgemeinschaft (Sonderforschungsbereich 450) and from the Fonds der Chemischen Industrie. A. M. Weiner gratefully acknowledges support from the Alexander-von-Humboldt Stiftung.

M. Woerner's e-mail address is woerner@mbi-berlin.de.

*Permanent address, School of Electrical and Computer Engineering, Purdue University, West Lafayette, Indiana 47907.

## REFERENCES AND NOTES

1. T. Elsaesser, J. G. Fujimoto, D. A. Wiersma, and W. Zinth, eds., *Ultrafast Phenomena XI* (Springer-Verlag, Berlin, 1998).
2. C. Chudoba, E. T. J. Nibbering, and T. Elsaesser, "Site-specific excited-state solute–solvent interactions probed by femtosecond vibrational spectroscopy," Phys. Rev. Lett. **81**, 3010–3013 (1998).
3. E. J. Heilweil, "Ultrafast glimpses at water and ice," Science **283**, 1467–1468 (1999).
4. S. Woutersen, U. Emmerichs, and H. J. Bakker, "Femtosecond mid-IR pump–probe spectroscopy of liquid water: evidence for a two-component structure," Science **278**, 658–660 (1997).
5. P. Hamm, M. Lim, and R. Hochstrasser, "Non-Markovian dynamics of the vibrations of ions in water from femtosecond infrared three-pulse photon echoes," Phys. Rev. Lett. **81**, 5326–5329 (1998).
6. R. M. Hochstrasser, P. Hamm, and M. Lim, "Femtosecond Dynamics, two-dimensional infrared spectroscopy and echoes of protein vibrations," in *Ultrafast Phenomena XI*, T. Elsaesser, J. G. Fujimoto, D. A. Wiersma, and W. Zinth, eds. (Springer-Verlag, Berlin, 1998), pp. 653–657.
7. T. Elsaesser and M. Woerner, "Femtosecond infrared spectroscopy of semiconductors and semiconductor nanostructures," Phys. Rep. **321**, 253–305 (1999).

8. R. A. Kaindl, S. Lutgen, M. Woerner, T. Elsaesser, B. Nottelmann, V. M. Axt, T. Kuhn, A. Hase, and H. Künzel, "Ultrafast dephasing of coherent intersubband polarizations in a quasi-two-dimensional electron plasma," Phys. Rev. Lett. **80**, 3575–3578 (1998).
9. S. Lutgen, R. A. Kaindl, M. Woerner, T. Elsaesser, A. Hase, H. Künzel, M. Gulia, D. Meglio, and P. Lugli, "Nonequilibrium dynamics in a quasi-two-dimensional electron plasma after ultrafast intersubband excitation," Phys. Rev. Lett. **77**, 3657–3660 (1996).
10. R. A. Kaindl, M. Woerner, T. Elsaesser, D. C. Smith, J. F. Ryan, G. A. Farnan, M. P. McCurry, and D. G. Walmsley, "Ultrafast mid-infrared response of $YBa_2Cu_3O_{7-\delta}$," Science **287**, 470–473 (2000).
11. A. Baltuska, Z. Wei, M. S. Pshenichnikov, and D. A. Wiersma, "Optical pulse compression to 5 fs at a 1-MHz repetition rate," Opt. Lett. **22**, 102–104 (1997).
12. M. Nisoli, S. DeSilvestri, O. Svelto, R. Szipöcs, K. Ferencz, Ch. Spielmann, S. Sartania, and F. Krausz, "Compression of high-energy laser pulses below 5 fs," Opt. Lett. **22**, 522–524 (1997).
13. R. L. Fork, C. H. BritoCruz, P. C. Becker, and C. V. Shank, "Compression of optical pulses to six femtoseconds by using cubic phase compensation," Opt. Lett. **12**, 483–485 (1987).
14. D. E. Spence, S. Wielandy, C. L. Tang, C. Bosshard, and P. Günter, "High-average power, high-repetition rate femtosecond pulse generation in the 1–5 $\mu$m region using an optical parametric oscillator," Appl. Phys. Lett. **68**, 452–454 (1996).
15. C. McGowan, D. T. Reid, M. Ebrahimzadeh, and W. Sibbett, "Femtosecond pulses tunable beyond 4 $\mu$m from a KTA-based optical parametric oscillator," Opt. Commun. **134**, 186–190 (1997).
16. V. Petrov and F. Noack, "Tunable femtosecond optical parametric amplifier in the mid-infrared with narrow-band seeding," J. Opt. Soc. Am. B **12**, 2214–2221 (1995).
17. G. M. Gale, G. Gallot, F. Hache, and R. Sander, "Generation of intense highly coherent femtosecond pulses in the mid-infrared," Opt. Lett. **22**, 1253–1255 (1997).
18. A. Lohner, P. Kruck, and W. W. Rühle, "Generation of 200 femtosecond pulses tunable between 2.5 and 5.5 $\mu$m," Appl. Phys. **59**, 211–213 (1994).
19. T. Elsaesser and M. C. Nuss, "Femtosecond pulses in the mid-infrared generated by downconversion of a traveling-wave dye laser," Opt. Lett. **16**, 411–413 (1991).
20. C. Ludwig, W. Frey, M. Woerner, and T. Elsaesser, "Generation of synchronized femtosecond pulses independently tunable in the mid-infrared," Opt. Commun. **102**, 447–451 (1993).
21. M. R. X. de Barros, R. S. Miranda, T. M. Jedju, and P. C. Becker, "High-repetition rate femtosecond mid-infrared pulse generation," Opt. Lett. **20**, 480–482 (1995).
22. V. Petrov, F. Rotermund, and F. Noack, "Femtosecond parametric generation in $ZnGeP_2$," Opt. Lett. **24**, 414–416 (1999).
23. F. Seifert, V. Petrov, and M. Woerner, "Solid state laser system for the generation of mid-infrared femtosecond pulses tunable from 3.3 to 10 $\mu$m," Opt. Lett. **19**, 2009–2011 (1994).
24. P. Hamm, M. Lim, and R. Hochstrasser, "Vibrational energy relaxation of the cyanide ion in water," J. Chem. Phys. **107**, 10523–10531 (1997).
25. J. M. Fraser, D. Wang, A. Haché, G. R. Allan, and H. M. van Driel, "Generation of high-repetition rate femtosecond pulses from 8 to 18 $\mu$m," Appl. Opt. **36**, 5044–5047 (1997).
26. S. Ehret and H. Schneider, "Generation of subpicosecond infrared pulses tunable between 5.2 and 18 $\mu$m at a repetition rate of 76 MHz," Appl. Phys. **66**, 27–30 (1998).
27. R. A. Kaindl, F. Eickemeyer, M. Woerner, and T. Elsaesser, "Broadband phasematched difference frequency mixing of femtosecond pulses in GaSe: experiment and theory," Appl. Phys. Lett. **75**, 1060–1062 (1999).
28. I. M. Bayanov, R. Danielus, P. Heinz, and A. Seilmeier, "Intense subpicosecond pulses tunable between 4 $\mu$m and 20 $\mu$m," Opt. Commun. **113**, 99–104 (1994).
29. T. Dahinten, U. Plödereder, A. Seilmeier, K. L. Vodopyanov, K. R. Allakhverdiev, and Z. A. Ibragimov, "Infrared pulses of 1 picosecond duration tunable between 4 $\mu$m and 18 $\mu$m," IEEE J. Quantum Electron. **29**, 2245–2250 (1993).
30. A. Dhirani and P. Guyot-Sionnest, "Efficient generation of infrared picosecond pulses from 10 to 20 $\mu$m," Opt. Lett. **20**, 1104–1106 (1995).
31. P. Y. Han and X.-C. Zhang, "Coherent broadband mid-infrared terahertz beam sensors," Appl. Phys. Lett. **73**, 3049–3051 (1998).
32. A. Bonvalet, M. Joffre, J. L. Martin, and A. Migus, "Generation of ultrabroadband femtosecond pulses in the mid-infrared by optical rectification of 15 fs light pulses at 100 MHz repetition rate," Appl. Phys. Lett. **67**, 2907–2909 (1995).
33. M. Joffre, A. Bonvalet, A. Migus, and J. L. Martin, "Femtosecond diffracting Fourier-transform infrared interferometer," Opt. Lett. **21**, 964–966 (1996).
34. A. Leitenstorfer, S. Hunsche, J. Shah, M. C. Nuss, and W. H. Knox, "Detectors and sources for ultrabroadband electro-optic sampling: experiment and theory," Appl. Phys. Lett. **74**, 1516–1518 (1999).
35. V. G. Dmitriev, G. G. Gurzadyan, and D. N. Nikogosyan, *Handbook of Nonlinear Optical Crystals*, Vol. 64 of Springer Series in Optical Sciences (Springer-Verlag, Heidelberg, Germany, 1997).
36. G. B. Abdullaev, L. A. Kulevskii, A. M. Prokhorov, A. D. Savel'ev, E. Y. Salaev, and V. V. Smirnov, "GaSe, a new effective material for nonlinear optics," JETP Lett. **16**, 90–92 (1972).
37. One type of these dichroic mirrors has high reflection at the pump wavelength (i.e., from 750 to 850 nm) and high transmission at the signal (1200–1620 nm). The other type has high reflection for the *s*-polarized signal and high transmission for the *p*-polarized idler (1620–2500 nm).
38. D. R. Suhre, N. B. Singh, V. Balakrishna, N. C. Fernelius, and F. K. Hopkins, "Improved crystal quality and harmonic generation in GaSe doped with indium," Opt. Lett. **22**, 775–777 (1997).
39. S. Akhmanov, A. S. Chirkin, K. N. Drabovich, A. I. Kovrigin, R. V. Khokhlov, and A. P. Sukhorukov, "Nonstationary nonlinear optical effects and ultrashort light pulse formation," IEEE J. Quantum Electron. **4**, 598–605 (1968).
40. A. M. Weiner, J. P. Heritage, and E. M. Kirschner, "High-resolution femtosecond pulse shaping," J. Opt. Soc. Am. B **5**, 1563–1572 (1988).
41. O. E. Martinez, "3000-times grating compressor with positive group velocity dispersion," IEEE J. Quantum Electron. **23**, 59–64 (1987).
42. J.-C. Diels and W. Rudoph, *Ultrashort Laser Pulse Phenomena: Fundamentals, Techniques, and Applications on a Femtosecond Timescale* (Academic, San Diego, Calif., 1996).
43. The adjustment is uncritical, because displacements of lens or grating necessary to induce a lengthening of a 100-fs pulse by a factor of 1.4 (i.e., one dispersion length) are of the order of 1 cm for a 150 line/mm grating and thus are easily controlled.
44. R. L. Fork, O. E. Martinez, and J. P. Gordon, "Negative dispersion using pairs of prisms," Opt. Lett. **9**, 150–152 (1984).
45. J. P. Heritage, A. M. Weiner, and R. N. Thurston, "Picosecond pulse shaping by spectral phase and amplitude modulation," Opt. Lett. **10**, 609–611 (1985).
46. A. M. Weiner, D. E. Leaird, J. S. Patel, and J. Wullert, "Programmable femtosecond pulse shaping by use of a multielement liquid-crystal phase modulator," Opt. Lett. **15**, 326–328 (1990).
47. A. M. Weiner, "Femtosecond pulse shaping using spatial light modulators," Rev. Sci. Instrum. **71**, 1929–1960 (2000).